Journal of Electroceramics, 9, 101–110, 2002

Cationic Surface Segregation in Donor-Doped $SrTiO_3$ Under Oxidizing Conditions

RENÉ MEYER,[1] RAINER WASER,[1] JULIA HELMBOLD[2] & GÜNTER BORCHARDT[2]

[1]*Institut für Werkstoffe der Elektrotechnik II, Aachen University, Germany*
[2]*Institut für Metallurgie, TU Clausthal, Germany*

Submitted March 26, 2002; Revised October 30, 2002; Accepted November 12, 2002

Abstract. The influence of high temperature oxygen annealing on (100) oriented donor-doped $SrTiO_3$ single crystals was studied. Crystalline precipitates were found on the optical scale on surfaces of lanthanum-doped as well as niobium-doped specimens with donor concentrations above 0.5 at.%. The amount of the secondary phase increases with the doping level, oxidation temperature and oxidation time. EDX analyses of the crystallites reveal a SrO_x composition.

The formation of the observed secondary phase is discussed by means of the defect re-equilibration of the cation sub-lattice. In view of the point defect model for donor-doped perovskites, n-conducting $SrTiO_3$ changes its compensation mechanism during an oxidation treatment from "electronic compensation" ($N_D = n$) to "self-compensation" ($N_D = 2[V''_{Sr}]$) by forming cation vacancies. Due to the favored Schottky-type disorder in perovskites, the formation of strontium vacancies is accompanied by a release of strontium from the regular lattice. Since the excess strontium is found to be situated at the surface in form of SrO-rich precipitates only, we propose the formation of strontium vacancies via a surface defect reaction and the chemical diffusion of strontium vacancies from the surface into the crystal as the most probable re-equilibration mechanism for the oxidation treatment of single crystals.

The introduced mechanism is in contrast to an established model which proposes the formation of Ruddlesden-Popper intergrowth phases $SrO{\cdot}(SrTiO_3)_n$ in the interior of the crystal.

Keywords: perovskite, donor, cation vacancy diffusion, SrO secondary phase, Ruddlesden-Popper phases

1. Introduction

Depending on the sintering atmosphere, donor-doped $SrTiO_3$ ceramics show either insulating or semiconducting properties. The drastic influence on the electrical conductivity is attributed to different compensation mechanisms of the excess positive charge of donor atoms. Reducing sintering conditions promote compensation by electrons in the conduction band that is formed from overlapping Ti $3d^1$ orbitals. Such processed materials reveal n-type conductivity. In chemical notation, Ti^{4+} is reduced to Ti^{3+}, whereby the electron is delocalized and contributes to the conduction process. In the following, we name this state "electronic compensation". High oxygen activities favor the formation of acceptor-like metal vacancies. In this case, electrons released from donor states are trapped by these intrinsic acceptor centers and lead to an ionic self-compensation of the material. The perovskite becomes an insulator and only Ti^{4+} ions exist in the crystal. In the following, this state is called "cation vacancy compensation".

The synthesis of single phase lanthanum doped strontium titanate was extensively studied by Moos et al. [1]. With respect to the sintering atmosphere, the compositions of secondary phase free perovskites for A-site or B-site substitution, are described as follows:

A-site substitution (e.g. lanthanum)

$$(1-x){\cdot}\mathrm{SrO} + \mathrm{TiO_2} + x{\cdot}\mathrm{La} \overset{\text{red. conditions}}{\rightarrow} \left(\mathrm{Sr}^{2+}_{1-x}\mathrm{La}^{3+}_{x}\right)\left(\mathrm{Ti}^{4+}_{1-x}\mathrm{Ti}^{3+}_{x}\right)\mathrm{O}^{2-}_{3} \quad (1)$$

$$(1-1.5x)\cdot\mathrm{SrO}+\mathrm{TiO_2}+x\cdot\mathrm{La}\xrightarrow{\text{ox. conditions}}\left(\mathrm{Sr}^{2+}_{1-1.5x}\square_{0.5x}\mathrm{La}^{3+}_{x}\right)\mathrm{Ti}^{4+}\mathrm{O}^{2-}_{3}\quad(2)$$

B-site substitution (e.g. niobium)

$$\mathrm{SrO}+(1-x)\cdot\mathrm{TiO_2}+x\cdot\mathrm{Nb}\xrightarrow{\text{red. conditions}}\mathrm{Sr}^{2+}\left(\mathrm{Ti}^{4+}_{1-2x}\mathrm{Ti}^{3+}_{x}\mathrm{Nb}^{5+}_{x}\right)\mathrm{O}^{2-}_{3}\quad(3)$$

$$(1-0.5x)\cdot\mathrm{SrO}+(1-x)\cdot\mathrm{TiO_2}+x\cdot\mathrm{Nb}\xrightarrow{\text{ox. conditions}}\left(\mathrm{Sr}^{2+}_{1-0.5x}\square_{0.5x}\right)\left(\mathrm{Ti}^{4+}_{1-x}\mathrm{Nb}^{5+}_{x}\right)\mathrm{O}^{2-}_{3}\quad(4)$$

According to Eqs. (2) and (4), a strontium deficit ($\square \mathrel{\hat{=}}$ *strontium vacancy*) has to be considered under oxidizing conditions in the composition to avoid the formation of SrO-rich second phases. However, it can be expected that a transition from one state to another also occurs at high temperatures. An oxidation of electronically compensated material according to Eqs. (1) and (3) may then lead to the creation of strontium vacancies and the additional formation of a SrO-rich second phase. A change from the "electronic compensation" to the "cation vacancy compensation" should follow Eq. (5) for lanthanum-doped or Eq. (6) for niobium-doped materials, respectively:

$$\mathrm{Sr_{1-x}La_xTiO_3}+\frac{\delta}{2}\mathrm{O_2}(g)\xrightarrow{\text{ox.}}\mathrm{Sr_{1-(x+\delta)}\square_\delta La_xTiO_3}+\delta\cdot\mathrm{SrO_{second\ phase}}\quad(5)$$

$$\mathrm{SrTi_{1-x}Nb_xO_3}+\frac{\delta}{2}\mathrm{O_2}(g)\xrightarrow{\text{ox.}}\mathrm{Sr_{1-\delta}\square_\delta Ti_{1-x}Nb_xO_3}+\delta\cdot\mathrm{SrO_{second\ phase}}\quad(6)$$

Due to the favored Schottky-type disorder in perovskites, the formation of strontium vacancies is accompanied by a release of strontium from the regular lattice:

$$\square_{\mathrm{Sr}}\equiv\mathrm{SrO_{second\ phase}}\quad(7)$$

point defect chemistry — second phase formation

Only indirect evidence for this transition such as electrical and thermogravimetric charcterization has been reported in the literature [2–5]. Electrical properties of donor-doped perovskites have been intensively studied as a function of oxygen partial pressure ($p\mathrm{O_2}$) and temperature in view of the broad technological relevance

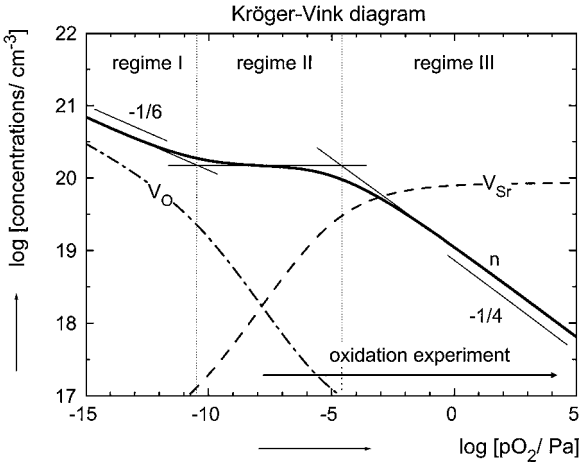

Fig. 1. Calculated defect concentrations of electrons, oxygen vacancies and strontium vacancies for a 1.0 at.% donor-doped single crystal as a function of $p\mathrm{O_2}$ at 1400°C. The arrow indicates the proposed change of the compensation mechanism from "electronic compensation" to "cation vacancy compensation". The study of this transition is the main issue of the present contribution.

of the material system. A set of mass action laws was developed and mass action constants were determined for a quantitative description via point defect equilibria [6]. Figure 1 shows the typical dependency of electrons (n), strontium vacancies (V_{Sr}) and oxygen vacancies (V_{O}) versus $p\mathrm{O_2}$ for a constant temperature in the Kröger-Vink diagram. Only under very reducing conditions (regime I), significant concentrations of oxygen vacancies are found. This regime will be excluded in the following. Regime II is characterized by a $p\mathrm{O_2}$ independent conductivity. Here, the concentration of electrons n is given by the donor N_D according to:

$$n\approx N_D\quad(8)$$

In regime III, the conductivity decreases with increasing oxygen activity. The formation of twice ionized strontium vacancies V''_{Sr} with acceptor character leads to a self-compensation of the material. Here, the concentration of electrons is given by:

$$n=N_D-2[V''_{\mathrm{Sr}}]\quad(9)$$

In thermodynamic equilibrium, the maximum concentration of strontium vacancies and hence, the maximum excess strontium is given by the amount of the

donor:

$$[V''_{\mathrm{Sr}}]_{\max} = \mathrm{Sr}_{\mathrm{excess}} \approx 0.5 \times N_D \tag{10}$$

The defect model provides a consistent description of the electrical behavior of the material by the introduced point defects. The conductivity σ is regarded as a sensitive indicator for the concentration of electrons and indirectly the concentration of strontium vacancies:

$$\sigma(p\mathrm{O}_2, T) = e_0 \times \mu_n \times n(p\mathrm{O}_2, T), \tag{11}$$

whereby e_0 denotes the elementary charge. In addition, the mass increase that should take place by the formation of strontium vacancies via an oxygen uptake according to Eqs. (12) and (13), was verified by thermogravimetry for ceramics [3] as well as powders [5].

$$\mathrm{Sr}_{\mathrm{Sr}} + \frac{1}{2}\mathrm{O}_2(g) + 2e' \overset{\mathrm{ox}}{\rightarrow} V''_{\mathrm{Sr}} + \mathrm{SrO}_{\text{second phase}} \tag{12}$$

$$\frac{\Delta m}{m} = \frac{n(\mathrm{Sr}_{1-x}\mathrm{La}_x\mathrm{TiO}_{3+0.5x}) - n(\mathrm{Sr}_{1-x}\mathrm{La}_x\mathrm{TiO}_3)}{n(\mathrm{Sr}_{1-x}\mathrm{La}_x\mathrm{TiO}_3)} \tag{13}$$

While electrical and thermogravimetric experiments give strong evidence for the formation of strontium vacancies, a direct observation of the postulated excess strontium has not been mentioned. Instead, growth of Ruddlesden-Popper (RP) phases $\mathrm{SrO}\cdot(\mathrm{SrTiO}_3)_n$ [7] that are known from the preparation of SrTiO_3 powders with large excess of SrCO_3, has been proposed in the $(\mathrm{SrLa})\mathrm{TiO}_3$ system [2, 5]. An experimental proof for this type of second phase, formed in a high temperature oxygen annealing step, has not yet been given.

So far, special attention was paid to equilibrated systems. Present research is dealing with the kinetics of transition [2–4, 8]. The nature of the re-equilibration process is still under investigation. Concerning this topic, we regard the destination of the excess strontium as the main question at present. In our last few publications, we reported on the direct observation of a SrO_x second phase on a single crystal surface [9, 10]. In this Letter, we studied the influence of doping concentrations and doping types (A, B-site) on the accumulation of strontium at the surface. On the basis of the presented experimental results, we propose a mechanism that is founded on the diffusion of strontium vacancies as the rate limiting process in the re-equilibration of the cation sub-lattice.

2. Experimental

(100) oriented single crystals, with commercial surface finish (Crystec GmbH, Berlin, Germany), were annealed in pure oxygen or air, respectively. For A-site substitution, 0.1 at.% La, 1.0 at.% La and 5.0 at.% La doped specimen were investigated. B-site substitutions

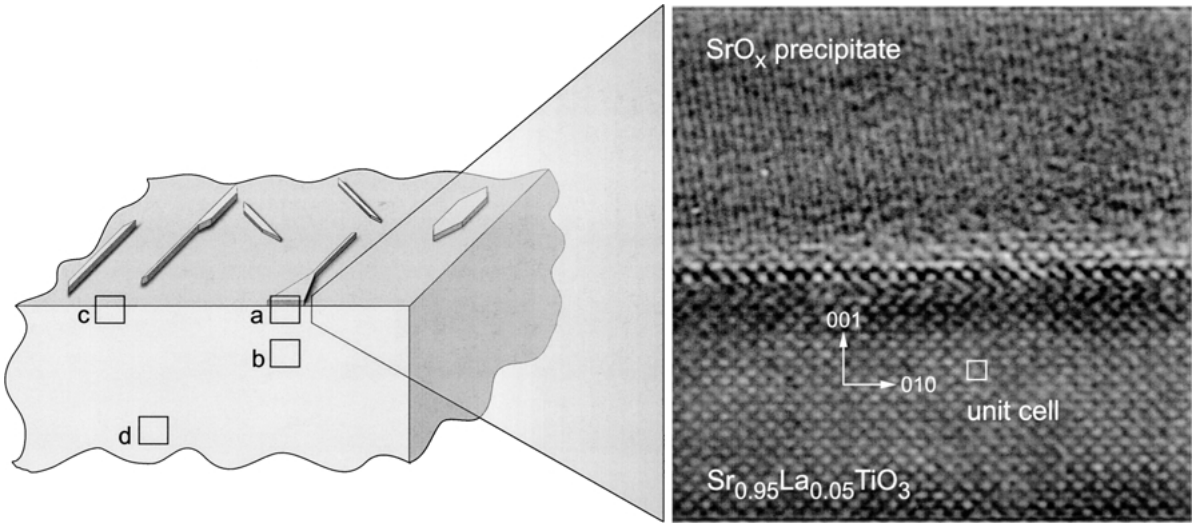

Fig. 2. HRTEM study of the perovskite/precipitate interface (a), the near-surface region in the vicinity of SrO second phases (b), the second phase free near-surface (c) and the crystal interior (d). No indications were found for the formation of Ruddlesden-Popper intergrowth phases.

were represented by 0.02 at.% Nb, 0.2 at.% Nb, 1.0 at.% Nb and 2.0 at.% Nb-doped samples. Dwell temperatures between 1050°C and 1350°C and annealing times between 10 h and 31 days were chosen. A temperature ramp of 5 K/min was used during the heating and cooling cycles. To make sure that the high temperature processing and not the cooling down is the important step in the experiment, some samples were also quenched to room temperature. Subsequently, the surface was investigated by optical microscopy. In addition, EDX analysis was carried out to identify secondary phases formed on the surface. Beside the standard SEM-EDX arrangement, insulated precipitates were investigated as well as TEM-EDX was applied to prevent a matrix contribution to the signal.

HRTEM analysis on oxidized single crystals was performed to study the formation of RP-phases in the vicinity of the surface as well as in the interior of the crystal. Care was taken during the sample preparation to prevent leaching effects of strontium. Characteristic locations (a–d) were chosen as illustrated in Fig. 2 to study different regions of the sample. In detail, we investigated the perovskite/precipitate interface (a), the region in the perovskite below a precipitate close to the surface (b), the second phase free surface (c) and the region of the crystal far from the surface (d).

3. Results

Figures 3(a) and (b) show optical surface images with the typical formation of precipitates. All specimens were oxygen annealed for $t = 25$ h at $T_{\mathrm{Dwell}} = 1350°\mathrm{C}$ in a single oxidation run. Afterwards, the furnance was cooled at 5 K/min to room temperature. Along with the formation of precipitates, the color of all single crystals changed from deep blue to transparent light blue.

Further it was found that the formation of crystallites depends on the amount of dopant. On $SrTiO_3$:La 0.1 at.%, precipitates were not identified within optical resolution. $SrTiO_3$:La 1.0 at.% (Fig. 3(a)) crystals show needle shaped precipitates with (110) orientation to the substrate as well as 2-dimensional regularly shaped crystallites. On the surface of $SrTiO_3$:La 5.0 at.% samples (Fig. 3(b)), partly oriented as well as less oriented crystallites with irregular shape were detected. The height of the precipitates was determined by profilometry. The average structure height of $SrTiO_3$:La 5.0 at.% was about 500 nm and about 200 nm for

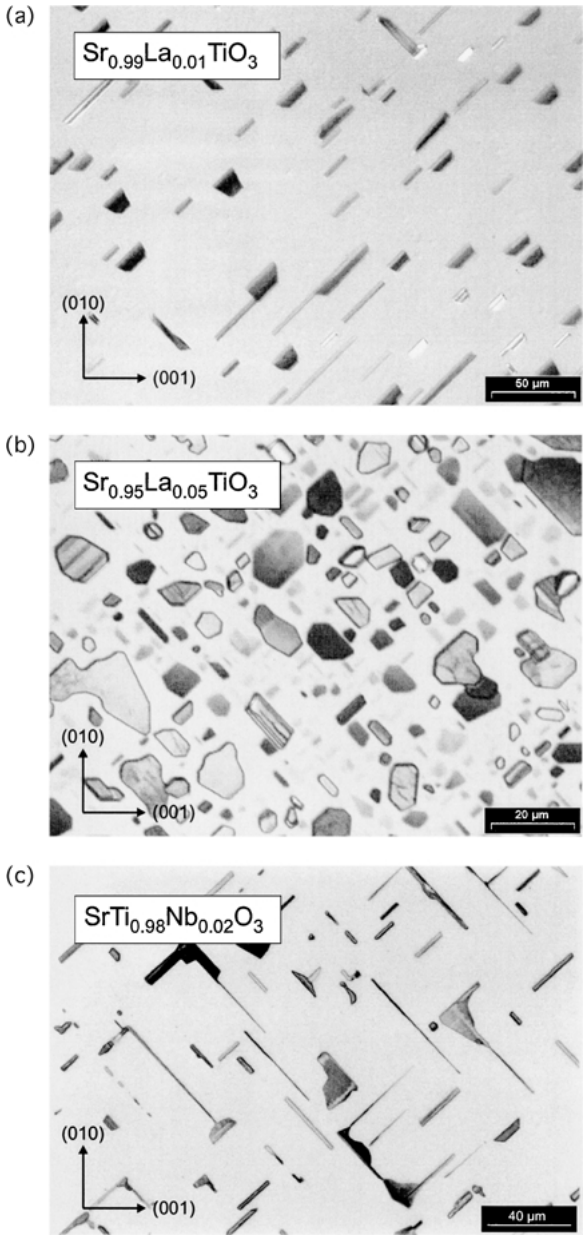

Fig. 3. Optical images of polished single crystal surfaces after oxygen annealing. Specimen with (a) 1.0 at.% lanthanum content and (b) 5.0 at.% lanthanum content were annealed at 1350°C for 25 h. For comparison, (c) shows a 2.0 at.% niobium-doped specimen annealed at 1300°C for 24 h.

$SrTiO_3$:La 1.0 at.% doped samples under the conditions applied.

For comparison Fig. 3(c) shows the surface of a $SrTiO_3$:Nb 2.0 at.% doped sample. This specimen was annealed in air for $t = 24$ h at a temperature of 1300°C

and subsequently quenched to room temperature. No significant difference was observed between niobium-doped and lanthanum-doped specimens with comparable amounts of doping.

EDX analyses (SEM-EDX and TEM-EDX) of the crystallites confirm the formation of SrO-rich second phases. Since the SrO stoichiometry could not be determined quantitatively by the applied methods, in the following sections, the second phase is denoted as SrO-rich or SrO_x, respectively. Lanthanum or niobium were not found. Therefore, a migration of the donor out of the crystal could be excluded. Further, no evidence was observed, which indicated any oxidation driven change of the matrix stoichiometry. Second phase-free parts of the surface and the reference crystals reveal the same composition within the experimental error.

Additional information about the crystallographic structure was deduced from the preferential (110)-oriented growth of the second phase. In (110) direction, the lattice parameter of $SrTiO_3$ is known to be 5.52 Å. Cubic SrO has a lattice constant of 5.16 Å. Considering stoichiometric SrO at the interface, an epitaxial growth of SrO on the $SrTiO_3$ substrate might be expected, since this configuration reveals a small lattice mismatch <7%. The approach is supported by investigation of Tambo et al. on epitaxial growth of $SrTiO_3$ on SrO surfaces [11].

Several temperatures were chosen to study the kinetics of crystallite formation. At temperatures below 1000°C, crystal surfaces do not yield crystallites within optical resolution. For AFM studies of undoped $SrTiO_3$ within this temperature range we refer to publications of Szot and Speier [12]. Above this temperature, the growth rate of the precipitates increases with temperature and with annealing time. Figure 4 shows the growth of precipitates on samples doped with 5.0 at.% lanthanum, annealed in air at 1300°C for 1 or 8 days, respectively, and quenched to room temperature. After one day, only small precipitates were found on the surface. Prolongated annealing caused a growth of the precipitates and an increase of the crystallite volume.

Even after extensive oxidation, the new equilibrium was not achieved. An estimation of the diffusion length of strontium vacancies under the applied conditions in the sub-mm range supports this observation [3].

To our surprise, no indications were found by HRTEM that point to a formation RP-phases in all of the regions studied (see Fig. 2). Only at the perovskite/precipitate interface, a lattice displacement of half a unit cell that could be attributed to the existence

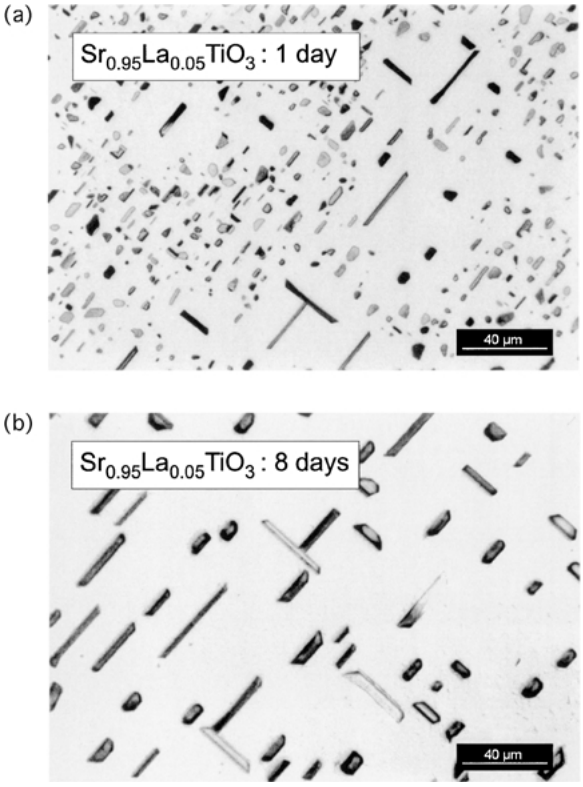

Fig. 4. Influence of the annealing time on the formation of SrO precipitates at the surface. In the illustration, 5.0 at.% lanthanum-doped single crystals were oxygen annealed in air at 1300°C for (a) 1 day or (b) 8 days, respectively.

of a RP phase in the topmost layer of the single crystal, was observed.

4. Discussion

4.1. Defect Configuration "As Grown"

The deep blue color of all single crystals before the heat treatment indicates a high concentration of Ti^{3+} [13]. The single crystals "as received" are situated in the electronic compensation (regime II). Since the relationship between doping concentration and electrons (or Ti^{3+}) is given by

$$n(=[Ti^{3+}]) \approx N_D, \tag{14}$$

the color intensity serves as an optical indicator for the conductivity. As expected, the intensity of the blue

color increases with the amount of doping. A sampling of the electrical properties confirms this statement. An estimation of point defect concentrations for growth temperatures provides similar results. Mass action coefficients were extrapolated from data obtained at high temperatures. Figure 5(a) illustrates the dependency of the strontium vacancy concentration on increasing temperature at a constant pO_2. The dashed lines indicate the approximated defect concentrations in the cation sub-lattice under growth conditions. Increasing the temperature shifts the cation defect equilibrium towards a lower concentration of cation vacancies. In addition, crystal growth under moderate reducing conditions is essential.

On the one hand, the cation vacancy versus temperature behavior shown in Fig. 5(a) seems to collide with the second law of thermodynamics that predicts an increase of point defects with rising temperature to minimize the Gibbs free energy in the system.

$$\Delta G = \Delta H - T \cdot \Delta S \tag{15}$$

On the other hand, donor-doped perovskites represent a complex system consisting of three charged particles (electrons, strontium vacancies, oxygen vacancies). Due to their charge, a concentration change of each defect type is restricted in terms of local electroneutrality. Hence, the minimization of the Gibbs free energy is a *collective phenomena* of all types of defects. The decrease in concentration of cation vacancies with increasing temperature, which was calculated from the point defect approach, has to be interpreted with regard to the above mentioned background. For the oxygen sub-lattice, an increase of point defects with rising temperatures as shown in Fig. 5(b) is predicted. To clarify the respective influence of the dopant on the point defect situation, similar defect calculations were also performed for undoped strontium titanate. In contrast to donor-doped $SrTiO_3$, simulation results reveal an increase of *both* anion and cation vacancies with increasing temperature. Concentrations versus temperature of the undoped system are plotted in Fig. 6(a) for oxygen vacancies and Fig. 6(b) for strontium vacancies.

When cooling down from growth temperatures, an increase of the cation vacancy concentration is expected as shown in Fig. 5(a), if the new thermodynamic equilibrium can be established. However, lower temperatures lead to decreasing defect mobilities and

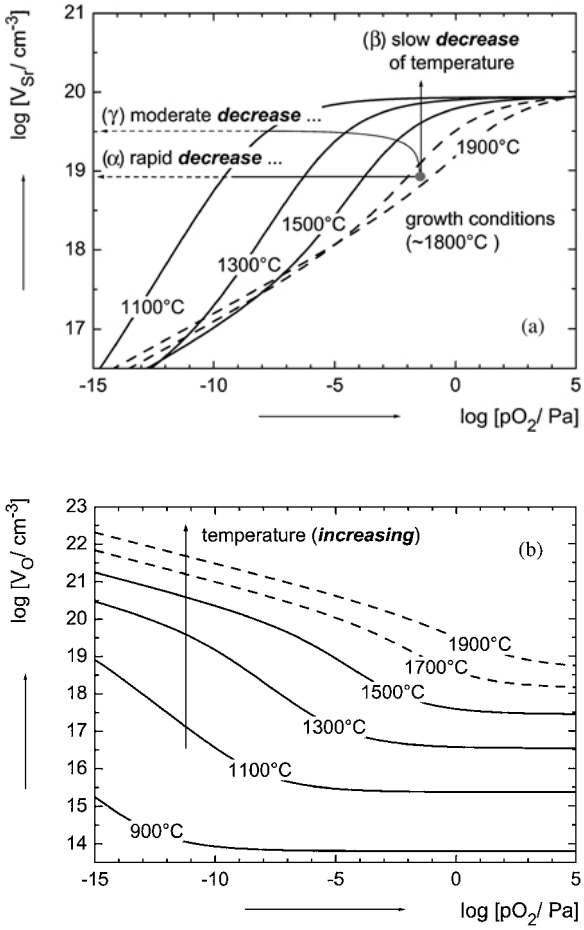

Fig. 5. (a) Calculated influence of temperature and pO_2 on the concentration of strontium vacancies for *n*-doped strontium titanate. Higher temperatures and lower oxygen activities show a similar effect. Surprisingly, the concentration of cation vacancies decreases with increasing temperature. Growth conditions for single crystals in the electronic compensation (regime II) are estimated from point defect reactions with respect to the electrical properties of the single crystals "as received" to clarify the defect situation before the experiment. The case of rapid cooling (α), very slow cooling (β) and intermediate cooling (γ, most realistic case) are discussed. As shown in the diagram, moderate oxygen activities are also essential to obtain n-type conducting material. (b) Calculated oxygen vacancy concentration versus pO_2 and temperature for donor-doped strontium titanate. An increase of temperature leads to an increase of anion site defects.

reaction rates. For kinetic reasons, the equilibrium non-stoichiometry inside the single crystal may only follow the new thermodynamic condition until a critical temperature × time product. Below, the density of ionic defects may not change and the sample ends

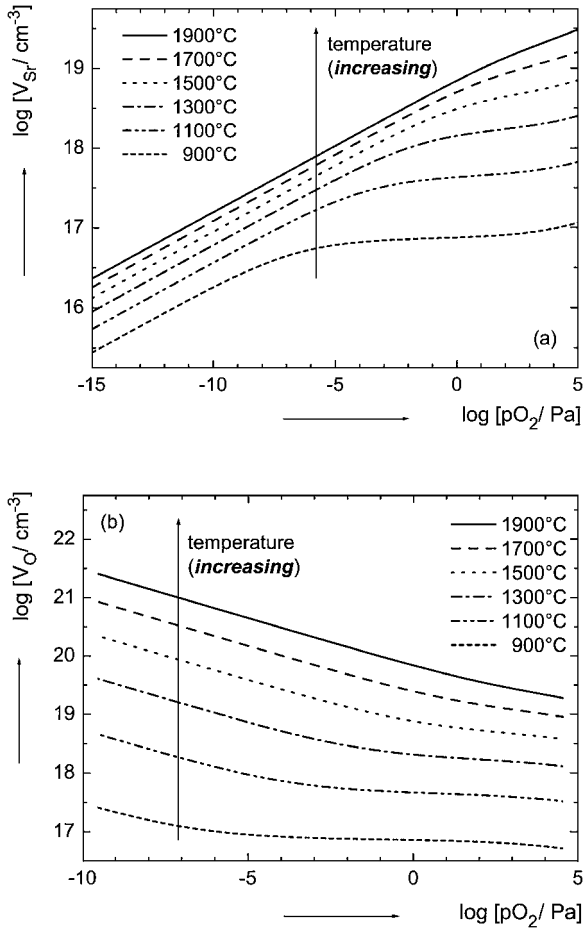

Fig. 6. Defect concentration of strontium vacancies (a) and oxygen vacancies (b) in undoped strontium titanate. In contrast to donor-doping, the concentration of both defect species increases with increasing temperature.

up in a meta stable state characterized by frozen-in non-equilibrium defect concentrations. Color as well as conductivity of the single crystal indicate that the defect concentrations of the so obtained single crystals are represented by region II in the Kröger-Vink-diagram.

When heated up once again in the experiment, the meta stable defect configuration now is driven to a new defect equilibrium state. Choosing oxidizing conditions, the point defect model predicts a change from the electron compensation (regime II) to the cation self compensation (regime III) as illustrated in Fig. 1.

4.2. Change of Color

After prolongated heat treatment under high pO_2, the color change to transparent blue indicates a shift of the oxidation state from Ti^{3+} to Ti^{4+}. This observation is consistent with predictions of the point defect model. The additional positive charge introduced by the valence change of titanium is compensated by strontium vacancies formed during the establishment of the new equilibrium.

4.3. Formation of SrO Precipitates

On lanthanum and niobium doped single crystals, SrO_x precipitates have formed on the surface after oxidation. Similar experimental findings, for A-site (lanthanum) or B-site (niobium) substitution with comparable amounts of dopant, point to an effect that correlates only with the doping concentration and is independent of the substitution site. Further, the amount of the observed SrO second phase scales with the doping content. Both results qualitatively correspond with predictions from the point defect reactions given by Eqs. (5) and (6). As we move from region II to region III of the sample, the expected volume of the SrO second phase may be estimated by:

$$\mathrm{SrO}_{\text{second phase}}(=[V''_{\mathrm{Sr}}]) \approx \frac{1}{2}N_D \qquad (16)$$

In Fig. 7, the amount of the expected second phase versus pO_2 is displayed in the logarithmic scale (a) and for the optical analysis, more importantly, in the linear scale (b). In the calculation, the doping concentration was varied between "undoped" and 5.0 at.%. We assume that for samples with doping content below 1.0 at.%, the amount for the second phase is below the optically detectable limit.

Second phase formation was only observed at the surface of the single crystals. HRTEM studies do not provide any indication for the establishment of RP-phases. We conclude that the re-equilibration process starts at the crystal surface. As a possible mechanism, we propose a near-surface formation of strontium vacancies followed by an in-diffusion. Time and temperature dependence support this suggestion. The formation process is assumed to be fast. The slow diffusion is attributed to be the rate limiting step in the sample re-equilibration.

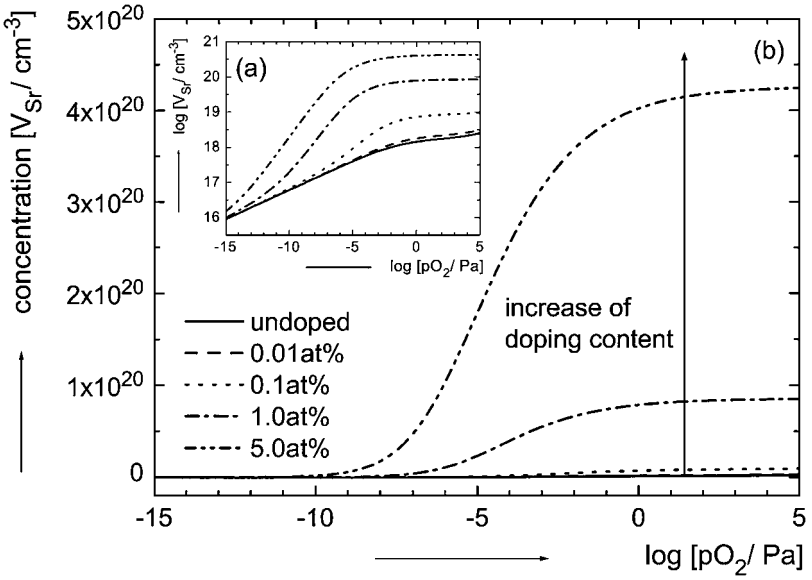

Fig. 7. Logarithmic (a) and linear (b) scale of the expected SrO second phase formation as a function of N_D according to point defect considerations. Only for donor concentrations $\geqq$1 at.%, a significant amount of strontium is expected to be released out of the crystal and to form precipitates at the surface.

4.4. Temperature Limit for the Formation of Precipitates

Second phase formation was only observed at temperatures above 1000°C. At temperatures below 1000°C, formation of precipitates was not accessible to optical resolution limits. In this temperature range, termination of the surface with a SrO layer on the atomic scale after heating under oxidizing conditions has been reported [12]. Apparently, strontium vacancies can even be formed at the surface, if the defect mobility is too low to diffuse into the crystal. The surface mobility of SrO complexes is regarded as high [14].

4.5. Proposed Model

On the basis of our experimental results, combined with literature data below 1000°C, we propose the following surface reconstruction mechanism. The initial surface is partly terminated with SrO and TiO_2 layers (Fig. 8(a)). At temperatures below 1000°C, strontium vacancies and SrO are formed at the surface (Fig. 8(b)) via the point defect reaction following Eqs. (5) or (6). The surface diffusion of highly mobile SrO complexes leads to a complete coverage of the surface with an atomic SrO layer. A significant volume diffusion of strontium vacancies does not occur, because in this temperature range, the mobility of cation vacancies is very low. Even at higher temperatures, strontium vacancies can be regarded as immobile for short term experiments. At temperatures above 1000°C and for prolongated oxidation in the range of days or weeks, a noticeable migration of strontium vacancies into the crystal as well as of strontium towards the surface takes place. According to the dependencies on time and temperature of the growth of the secondary phase, we propose a thermally activated vacancy diffusion mechanism (Fig. 8(c)). The excess SrO accumulates at the surface and crystallizes in (110) orientation in the observed SrO second phase. In view of this mechanism, the volume diffusion of strontium vacancies is the rate limiting step for the oxidation kinetics. The formation of strontium vacancies as a surface effect is regarded to be fast at elevated temperatures.

5. Summary

The influence of donor-doping and the substitution site (A-site or B-site) on the formation of a secondary phase in donor-doped $SrTiO_3$ was studied by optical microscopy. EDX analysis proved the second phases

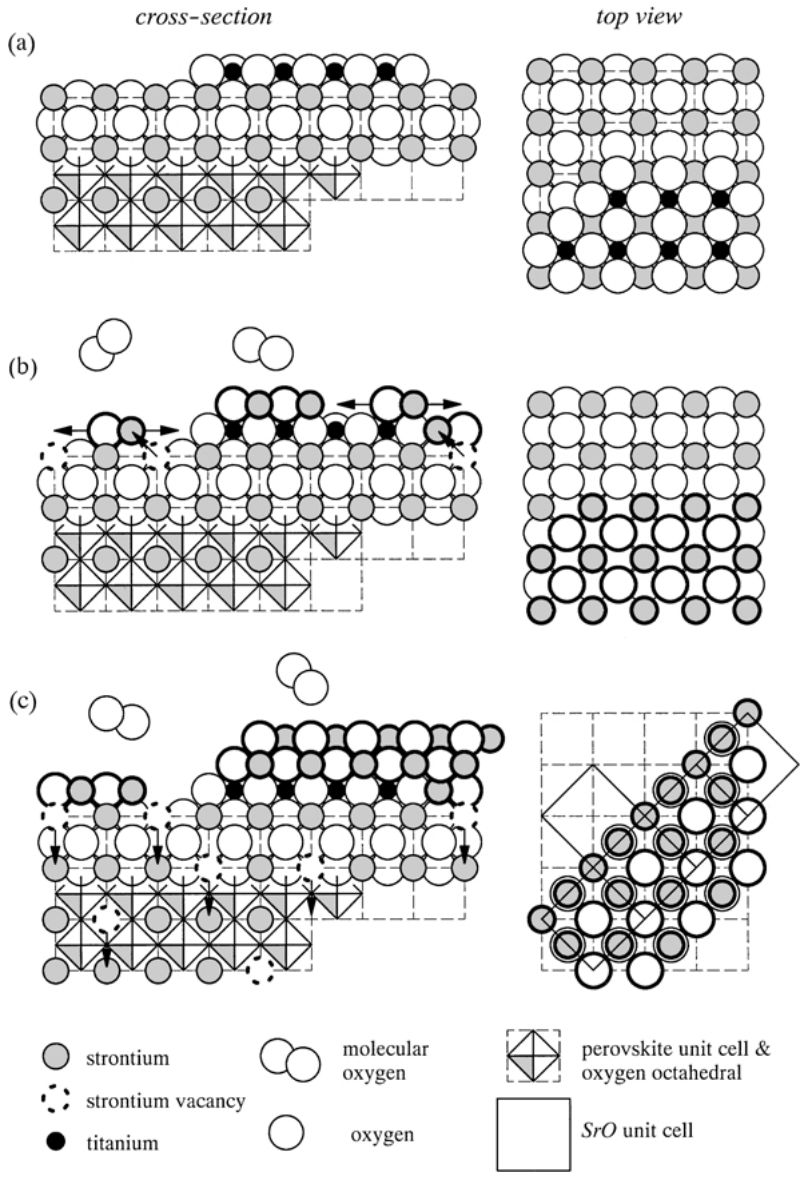

Fig. 8. (a) Cross-section and top view of the virgin crystal, based on the proposed model. Initially, a randomly SrO and TiO_2 terminated surface is assumed. (b) Upon exposing to high temperatures and oxidizing conditions, a formation of strontium vacancies takes place in the first monolayer according to a shift in the local point defect equilibrium of the cation sub-lattice. (c) An increase of temperature or long term experiments lead to a significant in-diffusion of strontium vacancies from the surface towards the interior of the crystal or a migration of strontium out of the sample, respectively. The excess strontium forms a SrO top-most layer over the whole crystal surface. Finally, epitaxial growth of SrO crystallites starts in (110)-orientation.

to consist of strontium and oxygen. Neither lanthanum nor niobium were found in the precipitates.

For doping concentrations equal or exceeding 1 at.%, it was shown that the amount of the second phase on top of the surface increases with the amount of dopant, the temperature and the oxidation time. No significant differences were found between lanthanum and niobium doped samples. The experimental results qualitatively confirm the point defect approach for donor-doped $SrTiO_3$, which predicts a linear relationship between the doping content and the amount of second phase ($N_D = 2[V''_{Sr}] = 2SrO$). Nevertheless, the time

dependence of the amount of the second phase indicates that thermodynamic equilibrium may not be reached in the experiment.

We propose an equilibration mechanism for the oxidation of the material that is based on the fast establishment of a local defect equilibrium at the surface and the slow in-diffusion of strontium vacancies. At temperatures below 1000°C, strontium vacancies and SrO complexes are formed in the first monolayer via a surface point defect reaction. At higher temperatures, the volume diffusion of strontium vacancies into the crystal causes an accumulation of SrO at the surface. The volume diffusion of strontium vacancies is regarded as the rate limiting step in the re-equilibration process.

No evidence has been found for the formation of Ruddlesden-Popper phases. Due to the lack of experimental proof, this mechanism does not seem to play a dominant role in the re-equilibration of the cation sub-lattice.

Our present studies focus on the influence of cation vacancies at the near-surface of single crystals or at grain boundaries in ceramics on the resistive properties of the material. Further, a numerical simulation program was developed to model the kinetics of diffusion of cation vacancies interacting with electronic and other ionic charge carriers [15–17].

Acknowledgments

We like to thank C.L. Jia from the Forschungszentrum Jülich for the HRTEM analysis. Special thanks for financial support are owed to the Deutsche Forschungsgemeinschaft (DFG).

References

1. R. Moos, T. Bischoff, W. Menesklou, and K.H. Härdtl, *Journal of Materials Science*, **32**, 4247 (1997).
2. R. Moos, Donatordotierungen in Strontiumtitanant: Elektrische Eigenschaften und modellhafte Beschreibung, PhD Thesis, Karlsruhe (Germany), VDI-Verlag Reihe 5, Nr. 362 (1994).
3. F. Poignant, L'oxydation de céramiques à base de titanate de strontium semi-conducteur et la formation de barrière de potentiel aux joints de grains, PhD Thesis, Limoges (France) (1995).
4. W. Menesklou, Kompensationsmechanismen der Überschußladung in lanthandotiertem Barium- und Strontiumtitanat, PhD Thesis, Karlsruhe (Germany), VDI-Verlag Reihe 5, Nr. 481 (1997).
5. N.G. Eror and U. Balachandran, *J. Sol. State Chem.*, **40**, 85 (1981).
6. R. Moos and K.H. Härdtl, *J. Am. Ceram. Soc*, **80**, 2549 (1997).
7. S.N. Ruddlesden and P. Popper, *Acta Crys.*, **11**, 54 (1957).
8. W. Menesklou, H.-J. Schreiner, K.H. Härdtl, and E. Ivers-Tiffée, *Sensors and Actuators* B, **59**, 184 (1999).
9. R. Meyer, K. Szot, and R. Waser, *Ferroelectrics*, **224**, 323 (1999).
10. J. Helmbold, G. Borchardt, R. Meyer, R. Waser, S. Weber, and S. Scherrer, *NATO ASI Series 3*, **77**, 461 (2000).
11. T. Tambo, T. Nakamura, K. Maeda, H. Ueba, and C. Tatsuyama, *Jpn. J. Appl. Phys.*, **37**, 3354 (1998).
12. K. Szot and W. Speier, *Phys. Rev.* B, **60**, 5909 (1999).
13. Holleman-Wiberg, edited by Nils Wiberg, 91–100 edition (De Gruyter, Berlin, 1985), p. 1065.
14. M. Kubo et al., *J. Chem. Phys.*, **109**, 8601 (1998).
15. R. Meyer and R. Waser, *J. Europ. Ceram. Soc.*, **21**, 1743 (2001).
16. R. Meyer, R. Waser, J. Helmbold, and G. Borchardt, *Phys. Rev. Lett.*, in press.
17. R. Meyer and R. Waser, unpublished results.